Cell Stem Cell
Short Article

Stage-Specific Roles for Tet1 and Tet2 in DNA Demethylation in Primordial Germ Cells

John J. Vincent,[1,2,3] Yun Huang,[7] Pao-Yang Chen,[2,3,8] Suhua Feng,[2,3] Joseph H. Calvopiña,[2,3] Kevin Nee,[2] Serena A. Lee,[2] Thuc Le,[4,5] Alexander J. Yoon,[1,5] Kym Faull,[1,5] Guoping Fan,[1,3,4] Anjana Rao,[7] Steven E. Jacobsen,[1,2,3,6] Matteo Pellegrini,[1,2,3] and Amander T. Clark[1,2,3,*]
[1]Molecular Biology Institute
[2]Department of Molecular, Cell, and Developmental Biology
[3]Eli and Edythe Broad Center of Regenerative Medicine and Stem Cell Research
[4]Department of Human Genetics
[5]Pasarow Mass Spectrometry Laboratory
[6]Howard Hughes Medical Institute
University of California, Los Angeles, Los Angeles, CA 90095, USA
[7]La Jolla Institute for Allergy & Immunology, La Jolla, CA 92037, USA
[8]Institute of Plant and Microbial Biology, Academia Sinica, Taipei 11529, Taiwan, ROC
*Correspondence: clarka@ucla.edu
http://dx.doi.org/10.1016/j.stem.2013.01.016

SUMMARY

Primordial germ cells (PGCs) undergo dramatic rearrangements to their methylome during embryogenesis, including initial genome-wide DNA demethylation that establishes the germline epigenetic ground state. The role of the 5-methylcytosine (5mC) dioxygenases Tet1 and Tet2 in the initial genome-wide DNA demethylation process has not been examined directly. Using PGCs differentiated from either control or *Tet2*$^{-/-}$; *Tet1* knockdown embryonic stem cells (ESCs), we show that in vitro PGC (iPGC) formation and genome-wide DNA demethylation are unaffected by the absence of Tet1 and Tet2, and thus 5-hydroxymethylcytosine (5hmC). However, numerous promoters and gene bodies were hypermethylated in mutant iPGCs, which is consistent with a role for 5hmC as an intermediate in locus-specific demethylation. Altogether, our results support a revised model of PGC DNA demethylation in which the first phase of comprehensive 5mC loss does not involve 5hmC. Instead, Tet1 and Tet2 have a locus-specific role in shaping the PGC epigenome during subsequent development.

INTRODUCTION

DNA methylation is an epigenetic mark involving the addition of a methyl group to the fifth carbon of a cytosine base (5mC). In mammalian cells, DNA methylation is established and maintained mostly in CG sequence contexts, and the amount of cytosine methylation in a given genome is relatively stable (Feng et al., 2010). Despite this stability, there are periods in embryonic development where DNA methylation is significantly reduced, including after oocyte fertilization, during preimplantation embryo development, and during primordial germ cell (PGC) formation (Gkountela et al., 2012; Guibert et al., 2012; Hackett et al., 2013; Hajkova et al., 2008; Hajkova et al., 2002; Hajkova et al., 2010; Monk et al., 1987; Okano et al., 1999; Popp et al., 2010; Seisenberger et al., 2012; Seki et al., 2005; Smith et al., 2012). Recent work has revealed a critical role for the oxidation of 5mC to 5-hydroxymethylcytosine (5hmC) by *Tet methylcytosine dioxygenase 1* (*Tet1*) and *Tet2* in locus-specific DNA demethylation in PGCs (Yamaguchi et al., 2012; Hackett et al., 2013). However, a role for 5hmC in the initial widespread (global) depletion of DNA demethylation in PGCs has not been addressed (Figure 1A).

PGCs are the founder cells of the metazoan germline, and abnormal PGC development causes infertility or cancer. Mammalian PGCs are specified de novo in each generation from the epiblast (Lawson and Hage, 1994; Ohinata et al., 2006; Tam and Zhou, 1996; Ying et al., 2001) and begin as highly methylated cells (Seki et al., 2005). Although methylation is critical for lineage specialization (Lei et al., 1996), it poses an inherent problem for PGCs, which become globally depleted of DNA methylation by e13.5 (Guibert et al., 2012; Kafri et al., 1992; Monk et al., 1987; Popp et al., 2010). This differential has lead to a longstanding hypothesis that a loss of methylation in PGCs prior to e13.5 is necessary to restore the germline epigenetic ground state, but the mechanisms for this restoration are not well understood (Reik and Walter, 2001).

PGCs undergo DNA demethylation in two phases (Seisenberger et al., 2012) (Figure 1A). The first phase involves global depletion of cytosine methylation with the retention of locus-specific methylation at imprinting control centers (ICCs), single copy genes, and repetitive elements (Guibert et al., 2012; Hackett et al., 2013; Hajkova et al., 2002; Lane et al., 2003; Lees-Murdock et al., 2003; Seki et al., 2005). The second phase occurs from e9.5 to e13.5, where methylation is depleted from the PGC genome in a locus-specific manner (Guibert et al., 2012; Hackett et al., 2013; Hajkova et al., 2008; Hajkova et al., 2002; Hajkova et al., 2010; Popp et al., 2010; Seisenberger et al., 2012; Yamaguchi et al., 2012). Recent work has revealed a role for Tet1 in the locus-specific demethylation of meiotic genes (Yamaguchi et al., 2012). However, given that 5hmC levels

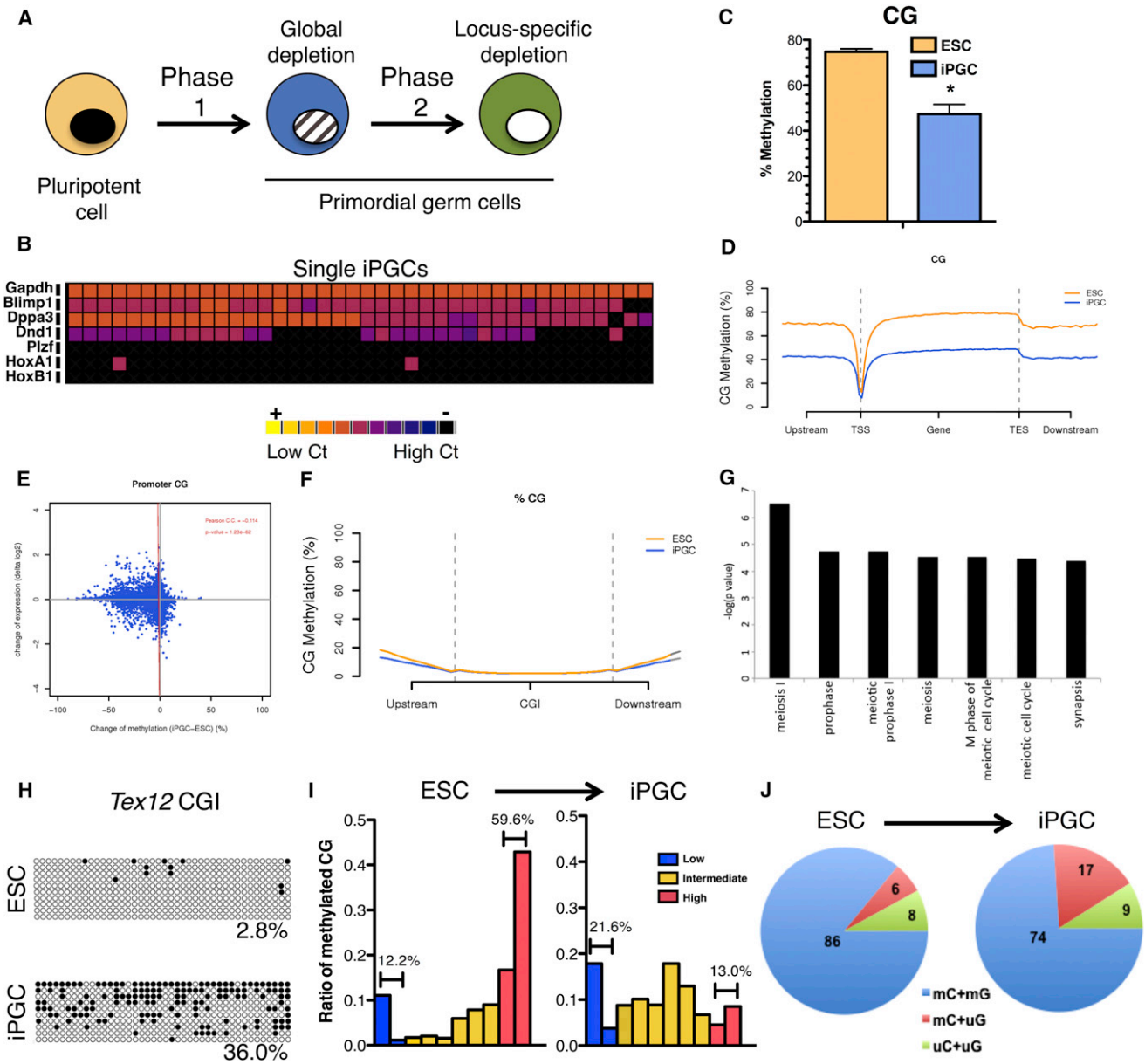

Figure 1. Generation of PGCs from ESCs Results in a Significant Decrease in CG Methylation

(A) A two-phase model of PGC demethylation is shown. PGCs are specified from pluripotent cells (yellow) and initially contain high levels of 5mC (black nucleus). In phase 1, PGCs younger than e9.5 (blue) undergo global DNA demethylation (Seisenberger et al., 2012). In phase 2, PGCs undergo locus-specific demethylation (white nucleus). Tet1 and Tet2 regulate locus-specific demethylation in phase 2 (Hackett et al., 2013). The role of Tet1 and Tet2 in global demethylation is unknown.

(B) Single cell analysis of sorted iPGCs.

(C) Quantification of cytosine methylation in the CG sequence context by BS-seq. Shown is mean ± SD (n = 3).

(D) Metaplot analysis of CG methylation at NCBI Reference Sequence (RefSeq) genes.

(E) Pearson analysis of differentially methylated sites (DMS) with gene expression.

(F) Metaplot of CG methylation at CG islands (CGIs).

(G) Gene ontology analysis of 100 CGIs with significantly higher methylation levels in iPGCs.

(H) Bisulfite PCR of *Tex12* CGI. Black circles, methylated cytosines; white circles, unmethylated cytosines.

(I) Distribution of cytosine methylation in ESCs and iPGCs. Binned bars representing 10% increments of methylation are graphed along the x axis.

(J) Frequency of methylation symmetry in CG sequence contexts in iPGCs after differentiation from ESCs. *, $p < 0.05$.

See also Figure S1 and Tables S1 and S2.

were reduced by only 45% in this model, it is conceivable that a second Tet protein may have compensated for loss of Tet1. More recently, a double knockdown of *Tet1* and *Tet2* in embryonic stem cell (ESC)-derived PGCs revealed a role for Tet1 and Tet2 in the demethylation of germline genes *Deleted in azoospermia-like* (*Dazl*), *Maelstrom* (*Mael*), and *Synaptonemal complex protein 3* (*Sycp3*) (Hackett et al., 2013). However, it was not determined whether Tet1 and Tet2 act to regulate global DNA demethylation in phase 1.

In the current study, our goal was to evaluate the role of Tet1 and Tet2 in genome-wide DNA demethylation by differentiating in vitro PGCs (iPGCs) from ESCs. It has previously been reported that this method robustly captures immature PGCs transcriptionally younger than e10.5 of development at high purity (Vincent et al., 2011). However, it is not known whether global DNA demethylation occurs in this model. Therefore, this study had two goals. The first goal was to examine whether the differentiation of iPGCs from ESCs involves a genome-wide depletion of DNA methylation from the iPGC genome and, if so, the second goal was to use this model to determine whether Tet1 and Tet2 regulate phase 1 genome-wide demethylation in PGCs.

RESULTS

PGCs undergo DNA demethylation in two phases (Seisenberger et al., 2012). In phase 1, 5mC is depleted globally from the genome with rare, locus-specific retention of methylation, including the ICC of *Snrpn* (Figures S1A–S1D available online). To determine whether ESC-derived iPGCs undergo genome-wide demethylation, we used two independently derived ESC lines (V6.5 and *Rosa26-GFP*) and differentiated iPGCs with embryoid body (EB) differentiation. The iPGCs were sorted on day 6 with surface markers stage-specific embryonic antigen 1 (SSEA1) and c-kit and then gated on the SSEA1^{+} and c-kit^{bright} double positive population (Figure S1F). The transcriptional identity of iPGCs was confirmed with single-cell gene expression analysis of 40 SSEA1^{+}c-kit^{bright} cells from the XY V6.5 background (Figure 1B). In this study, a higher cross threshold (Ct) indicated lower gene expression, and black indicated no detectable Ct and therefore no expression. We found that 38 of 40 iPGCs coexpressed the PGC genes *Blimp1* and *Dppa3* and that single iPGCs heterogeneously expressed *Dead end homolog 1* (*Dnd1*), as previously reported (Vincent et al., 2011). We also determined that the XY iPGCs do not express the spermatogonial marker *Plzf* and are negative for somatic lineage markers *Hoxa1* and *Hoxb1.* Using bisulfite (BS) treatment of iPGC DNA followed by PCR amplification of the *Snprn* ICC, we demonstrate that iPGCs on day 6 are methylated, indicating that iPGCs have not completed phase 2 demethylation (Figure S1E).

Next, we performed whole-genome BS sequencing (BS-seq) to compare cytosine methylation in ESCs and iPGCs (Table S1). Notably, BS treatment does not distinguish between 5mC and 5hmC (Huang et al., 2010). Therefore, the use of BS was for detecting the sum of 5mC and 5hmC. Cytosine methylation was mapped with the use of BS Seeker (Chen et al., 2010) with mouse genome build mm9 (UCSC Genome Browser) allowing up to three mismatches. Using this approach, we quantified a statistically significant ($p < 0.05$) reduction in the levels of CG methylation in iPGCs relative to ESCs (Figure 1C). Specifically, we determined that, on average, 75% of cytosines in a CG sequence context in ESCs were methylated, whereas, in iPGCs, this was reduced to 47%. Cytosine methylation was also observed in non-CG contexts. However, the amounts of non-CG methylation were low, at around 2% or less (Table S1). Though non-CG methylation in iPGCs trended toward depletion, this trend did not reach statistical significance.

To map genomic regions where a loss of CG methylation occurred, we sequenced undifferentiated ESCs to 6.8× and iPGCs to 6.9× coverage per strand, resulting in 478,482,437 cytosines covered $\geq$ 4× in both samples. Sites with delta methylation levels $\geq$ 30% were subject to two-way binomial tests, which yielded 11,994,107 CG sites for further analysis. We determined that 8,623,115 methylated cytosines in a CG sequence context were significantly decreased in iPGCs, whereas only 81,884 methylated cytosines in a CG sequence context were significantly increased in iPGCs relative to ESCs (FDR $\leq$ 5%). Chromosomal views of iPGCs in 1 million bp windows revealed a chromosome-wide depletion of CG methylation across all chromosomes (Figure S1G). Metaplots of reference genes showed typical depletion of CG methylation at the transcription start site (TSS) in both iPGCs and ESCs but general hypomethylation in iPGCs across all upstream and downstream regions (Figure 1D). Examination of repeat regions including nuclear elements (SINEs and LINEs) revealed a similar depletion in CG methylation (Figures S1H and S1I). Next, we used a Shannon entropy calculation to capture the heterogeneity of methylated cytosines between samples (Figure S1J). We found that the entropy was considerably higher in iPGCs in comparison to ESCs. This was true for genes, pseudogenes, exons, and introns. The one exception was gene promoters (defined as −800 bp to +200 bp of the TSS), where the entropy was almost equivalent between ESCs and iPGCs. Altogether, we conclude that the loss of cytosine methylation from iPGCs occurred genome-wide and that the increased entropy indicates that the iPGC population is heterogeneously (not synchronously) undergoing demethylation.

To determine whether global changes in cytosine methylation correlate with global changes in gene expression, we plotted differentially methylated CG sites (DMS) against the average change in gene expression between ESCs and iPGCs for each reference gene (Figure 1E). ESC and iPGC gene expression data were obtained from Vincent et al., 2011. A Pearson correlation coefficient for all comparisons revealed that the DMS at promoters, gene bodies, exons, and introns exhibited no correlation to either an increase or a decrease in gene expression in iPGCs relative to ESCs (Figures 1E and S1K). Unlike the majority of the PGC genome, analysis of CG islands (CGIs) revealed no change in the percentage of CG methylation (Figure 1F). However, a small number of promoter CGIs significantly gained methylation in iPGCs, and these were enriched in gene ontology groups associated with meiosis (Figure 1G and Table S2). This was confirmed by bisulfite PCR of the meiotic gene *Tex12* CGI (Figure 1H). Altogether, these data demonstrate that methylation at CGIs undergoes dynamic and unique reorganization with iPGC differentiation.

Next, we evaluated changes in the distribution of methylated CGs in ESCs and iPGCs by mapping methylation levels

from 0% to 100% as a fraction of total cytosine methylation (Figure 1I). Cytosine methylation in ESCs exhibited a typical bimodal distribution where 59.6% of cytosines had ≥80% methylation (red, high), whereas 12.2% of cytosines had ≤ 20% methylation (blue, low). In contrast, in iPGCs, we observed a substantial loss of cytosine methylation from the high category and a near doubling of cytosines in the low category (from 12.2% to 21.6%). The largest change between ESCs and iPGCs was in their progression to the intermediate category (yellow, > 0.2 and < 0.8), where methylation more than doubled (from 28.2% to 65.3%).

Finally, we evaluated the symmetry of cytosine methylation (Figure 1J). In this analysis, mC+mG refers to symmetrically methylated CG sites where the cytosine from both strands of DNA (with the opposite strand read as G) are methylated. Similarly, a symmetrically unmethylated site is represented by uC+uG. Our analysis shows that, when iPGCs are differentiated from ESCs, there is a loss in symmetrical methylation and a 3-fold increase in asymmetrical methylation (Figure 1J). Altogether, the differentiation of iPGCs from ESCs results in a genome-wide reduction in cytosine methylation similar to what was previously reported for immature PGCs in phase 1 (Seisenberger et al., 2012).

Tet Proteins and 5hmC Are Found in PGCs In Vivo and In Vitro

Given the role for Tet-mediated conversion of 5mC to 5hmC as an intermediate in locus-specific DNA demethylation (Hackett et al., 2013), we were interested in examining expression of *Tet* genes at a single-cell level in Oct4-GFP$^+$ PGCs at e9.25, e10.25, and e11.5 (Figures 2A–2D) as well as iPGCs sorted at day 6 of EB differentiation (Figure 2E). Quantitative RT-PCR and RNA sequencing have been used to evaluate Tet gene expression in Oct4-GFP$^+$ PGCs (Hajkova et al., 2010; Yamaguchi et al., 2012; Hackett et al., 2013); however, the heterogeneity between PGCs in sequential developmental ages has not been well defined. Single-cell analysis revealed that *Tet1* is expressed as early as e9.25, and it was detected in every *Dppa3*$^+$ PGC examined to e11.5. In contrast, *Tet2* was heterogeneously expressed at e9.25 and e10.25 (51% and 57% of cells, respectively). At e11.5, the number of *Tet2*$^+$ PGCs increased substantially to be expressed in almost every *Dppa3*$^+$ PGC along with *Tet1*. Unlike *Tet1* and *Tet2*, *Tet3* was expressed in rare *Dppa3*$^+$ PGCs at e11.5. The cytidine deaminase *Aid* was negative, suggesting that Aid does not act during this period. Comparably, by analyzing iPGCs, we discovered that 40 of 40 iPGCs expressed *Tet1* and that almost every single iPGC (39 of 40) also expressed *Tet2* (Figure 2E). Similar to PGCs from the embryo, we did not find *Aid* expression in iPGCs, and *Tet3* was rarely expressed (Figure 2E).

Given the expression of at least one or two *Tet* genes in PGCs, we analyzed 5hmC by immunostaining (Figures 2F and 2G). We used the commercially available 5hmC antibody that was previously confirmed as specifically recognizing 5hmC and not cytosine or 5mC (Iqbal et al., 2011). To confirm specificity, we transiently transfected 293T cells with a plasmid encoding the Tet1 catalytic domain, and a 5hmC-specific signal was only found in transfected cells (Figure S2A). Next, using this antibody, we show that 5hmC is present in e10.5 SSEA1$^+$ PGCs (arrow heads) at levels similar to somatic cells (Figure 2F). The expression of 5hmC was mostly uniform through the PGC nucleus. However, by e13.5, 5hmC exhibits a characteristic punctate pattern that overlaps with DAPI$^+$ pericentromeric heterochromatin (Figure S2B). Immunohistochemistry of sorted iPGCs and control SSEA1$^+$ undifferentiated V6.5 ESCs revealed 5hmC enrichment in both cell types (Figure 2G) (Ficz et al., 2011).

To quantify global levels of 5hmC and 5mC, we used combined liquid chromatography electro-spray ionization tandem mass spectrometry with multiple-reaction monitoring (LC-ESI-MS/MS-MRM) (Figures 2H and 2I). With the use of this technique, 5.1% of total cytosines in V6.5 ESCs were methylated (Figure 2H) in a manner consistent with our previous report (Le et al., 2011). Next, we found that the levels of 5mC in iPGCs were significantly reduced to an average of 2.5%, whereas 5mC levels in somatic cells from the same EB were 4.9%. Furthermore, V6.5 ESCs and iPGCs had a similar 5hmC to 5mC ratio wherein 5hmC is approximately 50-fold lower in abundance than 5mC (Figure 2I). In contrast, analysis of somatic cells from the EB at day 6 revealed a significant reduction in 5hmC relative to ESCs, as previously reported (Koh et al., 2011; Tahiliani et al., 2009). Altogether, the differentiation of iPGCs from ESCs is not associated with a significant reduction in 5hmC in comparison to somatic cells, and this suggests that iPGCs uniquely regulate 5hmC modification during differentiation.

Tet1 and Tet2 Do Not Regulate Genome-Wide Demethylation in iPGCs

Given that 5hmC is found on less than 1% of cytosines in undifferentiated ESCs and iPGCs and that *Tet1* and *Tet2* are coexpressed, we considered two alternate hypotheses for the role of Tet1 and Tet2 in phase 1 genome-wide DNA demethylation. First, we could hypothesize that 5mC oxidation by *Tet1* and *Tet2* is required for genome-wide DNA demethylation in iPGCs and that this is initiated extensively in immature PGCs during EB formation. Therefore, the small measureable amounts of 5hmC in iPGCs at day 6 would underestimate the total 5mC to 5hmC conversion that occurred. A second hypothesis could be that 5hmC plays no role in phase 1 DNA demethylation in iPGCs.

To address these possibilities, we designed an experiment to generate iPGCs from *Tet2*$^{-/-}$ ESCs transduced with a lentivirally (LV)-delivered small hairpin RNA (shRNA) against *Tet1* (shTet1 LV). We used this approach because iPGCs (and many endogenous PGCs) coexpress *Tet1* and *Tet2* (Figure 2E), and the depletion of *Tet1* and *Tet2* alone in ESCs results in only mild to moderate changes in 5hmC (Koh et al., 2011). We found no statistically significant difference in the percentage of iPGCs differentiated from *Tet2*$^{-/-}$ ESCs transduced with a control LV (*Tet2*$^{-/-}$; control LV) relative to *Tet2*$^{-/-}$ ESCs transduced with the *Tet1* shRNA LV (*Tet2*$^{-/-}$; shTet1 LV) (Figure 3A). To determine knockdown in sorted iPGCs, we used fluorescence-activated cell sorting (FACS) to isolate iPGCs and examined *Tet* gene expression by real-time PCR (Figure 3B). As a positive control for *Tet2*, we sorted iPGCs differentiated from V6.5 ESCs transduced with control LV (WT; control LV). *Tet1* RNA was successfully depleted up to 80% with shTet1 LV in iPGCs (Figure 3B). *Tet2* was undetectable in *Tet2*$^{-/-}$ ESCs, and *Tet3* levels were very low relative to Tet1 and were unchanged in

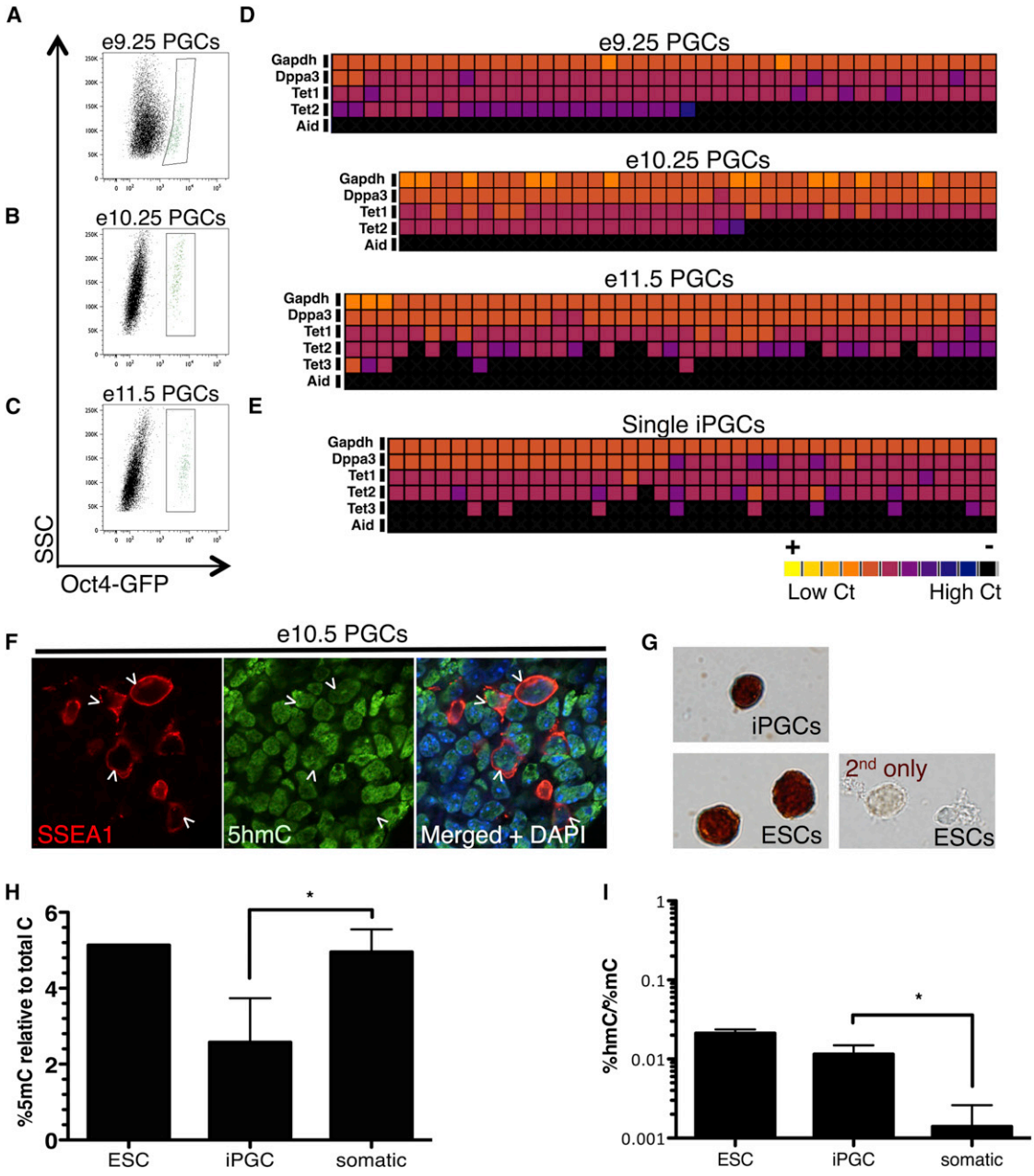

Figure 2. Tet1, Tet2, and 5-Hydroxymethylcytosine Are Present in PGCs and iPGCs

(A–C) FACS plots of GFP$^+$ PGCs (green) sorted from the mouse embryo at the indicated time points.

(D and E) Single-cell analysis of e9.25, e10.25, and e11.5 GFP$^+$ PGCs (D) and iPGCs (E) for *Tet1*, *Tet2*, *Tet3*, and *Aid*.

(F) Immunofluorescence of e10.5 PGCs for SSEA1 (red) and 5hmC (green).

(G) Immunohistochemistry for 5hmC in sorted day 6 iPGCs and undifferentiated ESCs. Control involves omitting the primary antibody.

(H and I) LC-ESI-MS/MS-MRM analysis of ESCs, iPGCs, and somatic EB cells for 5mC (H) and 5hmC (I) content. Shown are mean ± SD (n = 3). *, $p < 0.05$. See also Figures S1 and S2.

the context of *Tet2* deletion with or without *Tet1* knockdown (Figures 3B and 3C). Therefore, modulating Tet gene expression in iPGCs does not result in the compensatory expression of other Tet genes, similar to what was reported in undifferentiated ESCs (Dawlaty et al., 2011; Koh et al., 2011). We also analyzed the PGC-expressed genes *Blimp1* (a determinant of PGC fate), *Dppa3*, *Prdm14* (a determinant of PGC fate), and *Dnd1* and found that the manipulation of *Tet1* and *Tet2* had no significant effect on the expression of these genes relative to control genes (Figure 3D).

Finally, we asked whether *Tet1* and *Tet2* regulate genome-wide DNA demethylation with iPGC differentiation. If we accept the hypothesis that Tet1 and/or Tet2 are required for regulating genome-wide DNA demethylation, we would anticipate that

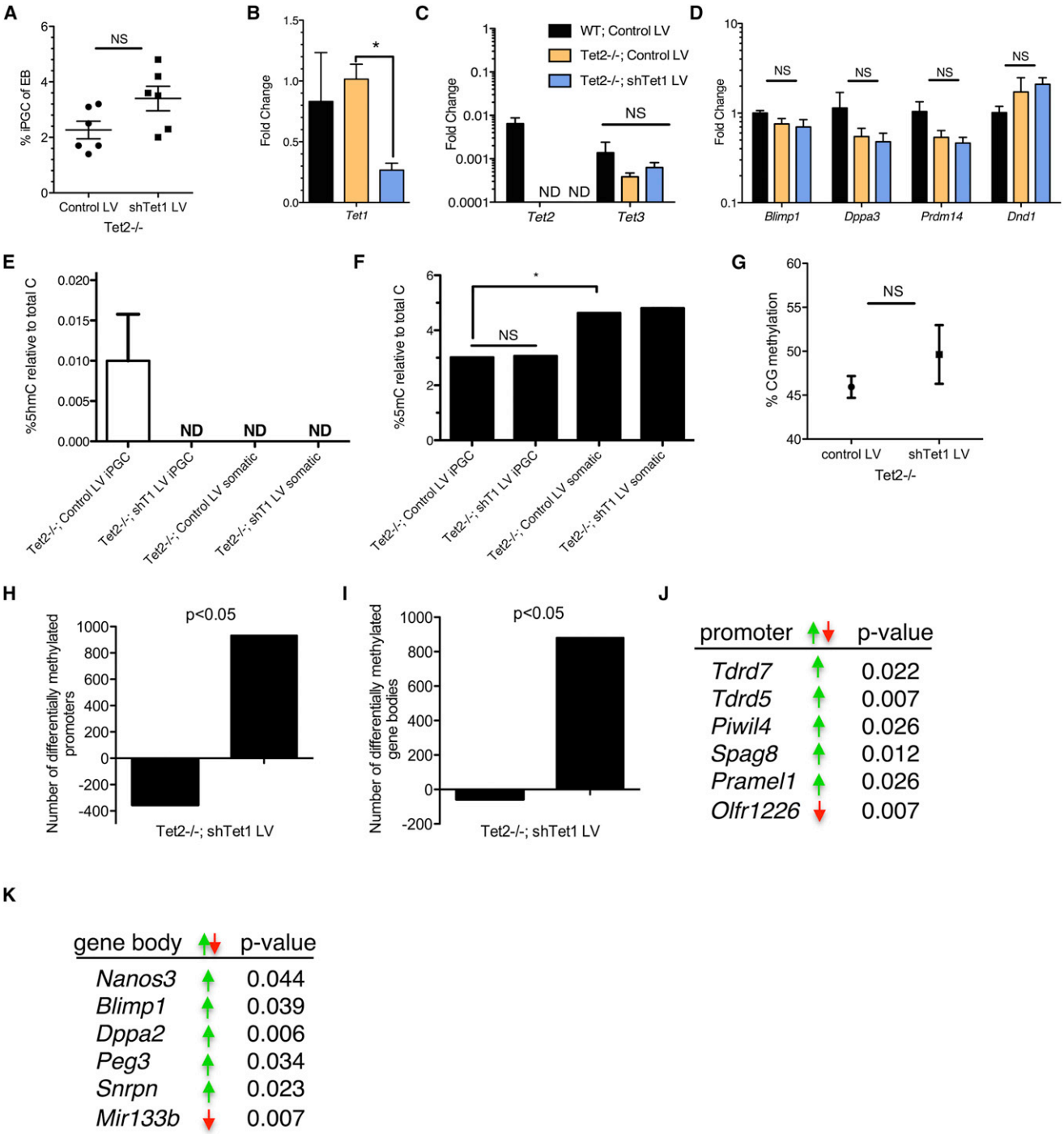

Figure 3. Tet1 and Tet2 Do Not Regulate Phase 1 Global DNA Demethylation in iPGCs

(A) The yield of iPGC differentiations in *Tet2*$^{-/-}$ cells transduced with a control lentivirus (LV) and an LV containing an shRNA against *Tet1* (shTet1 LV) (mean ± SEM of n = 6).

(B–D) The results of real-time PCR (mean ± SEM of n = 3).

(E and F) LC-ESI-MS/MS-MRM measurements for 5hmC (E) and 5mC (F) in iPGCs and somatic cells (mean ± SD of n = 3).

(G) Genome-wide CG methylation levels by BS-seq calculated from paired experiments (mean ± SEM of n = 3).

(H and I) The number of promoters (H) and gene bodies (I) that exhibit a statistically significant ($p < 0.05$) decrease (negative) or increase (positive) in CG methylation in *Tet2*$^{-/-}$; shTet1 LV PGCs.

(J and K) Promoters (J) and gene bodies (K) with differential methylation in *Tet2*$^{-/-}$; shTet1 iPGCs (green arrow, increase in methylation; red arrow, decrease in methylation). NS, not significant; ND, not detected; *, $p < 0.05$.

See also Figure S2 and Table S2.

cytosine methylation should significantly increase in *Tet2*$^{-/-}$; shTet1 LV iPGCs in comparison to *Tet2*$^{-/-}$; control LV. To reject the hypothesis and find that Tet1 and Tet2 have no major role in genome-wide iPGC demethylation, we would expect that *Tet2*$^{-/-}$; shTet1 LV iPGCs would have DNA methylation levels equivalent to wild-type iPGCs (Figure 1C). Using LC-ESI-MS/MS-MRM, we found that 5hmC was no longer detectable in *Tet2*$^{-/-}$; shTet1 iPGCs relative to *Tet2*$^{-/-}$; control LV (Figure 3E). We also found that, at the start of differentiation (day 6 posttransduction), the *Tet2*$^{-/-}$; shTet1 LV ESC samples had undetectable levels of 5hmC and no change in 5mC levels in comparison to *Tet2*$^{-/-}$; control LV (Figures S2C and S2D). Finally, analysis of 5mC by mass spectrometry revealed no increase in methylation in iPGCs with depleted 5hmC (Figure 3F). Thus, we conclude that *Tet1* and *Tet2* do not regulate global DNA demethylation.

Using an alternate approach, whole genome BS-seq in biological triplicate, we identified 6,866,888 CG dinucleotides that were represented in all six libraries, and, in agreement with the LC-ESI-MS/MS-MRM assay, we show no significant change in the percentage of CG methylation between *Tet2*$^{-/-}$; shTet1 LV iPGCs in comparison to *Tet2*$^{-/-}$; control LV iPGCs (Figure 3G). Combined, our data reject the first hypothesis that *Tet1* and *Tet2* regulate genome-wide DNA demethylation during iPGC differentiation. However, the BS-seq results reveal a small (~4%) increase in methylation in the Tet1 and Tet2 mutant iPGCs, which suggests locus-specific effects. Indeed, we found that knockdown of *Tet1* in a *Tet2*$^{-/-}$ background had a local effect on promoter and gene body methylation in iPGCs when compared to *Tet2*$^{-/-}$ iPGCs transduced with a control LV (Table S2). Importantly, the most significant directional change observed was CG hypermethylation in *Tet2*$^{-/-}$; shTet1 LV iPGCs in comparison to *Tet2*$^{-/-}$; control LV reference iPGCs (Figures 3H and 3I). Some notable hypermethylated promoters included the genome defense genes *Tudor domain containing protein 5* (*Tdrd5*) and *Piwi-like 4* (*Piwil4*), which are required to repress transposons later in germ cell development, and *Tdrd7*, *Spag8*, and *Pramel1*, which are expressed in adult testis (Figure 3J). Curiously, gene body hypermethylation was discovered on the germ cell-expressed genes *Nanos3*, *Blimp1*, and *Dppa2* and the imprinted genes *Peg3* and *Snrpn* (Figure 3K). However, the increase in gene body methylation at *Blimp1* did not alter expression (Figure 3D). We noted that olfactory receptor (*Olfr*) RNA and microRNAs (miRNAs) were highly represented in both promoter and gene body classifications, and shown here are an Olfr (*Olfr1226*) and a miRNA (*mir133b*) that exhibited hypomethylation in the *Tet1*- and *Tet2*-depleted iPGCs (Figures 3J and 3K). Altogether, this leads to a model where phase 1 PGC demethylation involving the bulk removal of DNA methylation is Tet1 and Tet2 independent.

DISCUSSION

Our genome-wide analysis of cytosine methylation with the use of BS-seq of iPGCs revealed a statistically significant and reproducible genome-wide depletion of cytosine methylation similar to what was recently reported by Seisenberger et al., 2012. Specifically, the iPGC model reported here captures the reorganization of cytosine methylation at meiotic CGIs relative to undifferentiated ESCs and represents a heterogeneous population of PGCs undergoing global phase 1 DNA demethylation and the initiation of some locus-specific, Tet-dependent DNA demethylation in phase 2. Although Tet1 and Tet2 were recently reported to regulate locus-specific demethylation in PGCs (Yamaguchi et al., 2012; Hackett et al., 2013), it was unknown whether the initial global depletion of DNA methylation required a 5hmC intermediate. Here, we show that Tet1, Tet2, and 5hmC are dispensable for the initial global depletion of 5mC from the PGC genome. Instead, Tet depletion induces promoter and gene body hypermethylation that is consistent with 5hmC having a locus-specific role in DNA demethylation in PGCs (Hackett et al., 2013).

Our genome-wide analysis reveals approximately 1,000 promoters and gene bodies that are differentially methylated in Tet1and Tet 2 mutant iPGCs, and the vast majority exhibit significant hypermethylation. Our data set revealed that *Dazl*, *Sycp3*, and *Mael* promoter methylation levels were all increased in the Tet1 and Tet2 mutants, as previously reported (Yamaguchi et al., 2012; Hackett et al., 2013). However, these changes did not reach statistical significance in our study, perhaps because the iPGCs here are younger than e10.5. One interesting observation was the discovery of important Tet-regulated germ cell-expressed genes, including *Tdrd5*, *Piwil4* (also called *Miwi2*), and *Tdrd7* that function in the male germline after e13.5 (Carmell et al., 2007; Tanaka et al., 2011; Yabuta et al., 2011). This suggests that 5hmC may prepare the germline epigenome for future functional events unique to this lineage.

If 5mC oxidation and deamination (Popp et al., 2010) are not responsible for driving genome-wide depletion in DNA demethylation in PGCs, what could be the mechanism? One possibility is that global demethylation is linked to abnormalities in replication-coupled methylation inheritance prior to e9.5. This could be caused by mislocalization, inactivation, or repression of *DNA methyltransferase 1* (*Dnmt1*) (Lei et al., 1996) or its cofactor *Uhrf1* during DNA synthesis (Bostick et al., 2007). Hairpin BS-seq (Laird et al., 2004), which detects methylation on complementary strands of DNA, is one way to address this in the ESC to iPGC model.

In conclusion, we propose that the differentiation of iPGCs represents a heterogeneous population of immature PGCs in the process of undergoing global genome-wide depletion of methylation during phase 1 and the beginning of Tet-dependent demethylation in phase 2. Our study demonstrates that Tet1 and Tet2 do not regulate initial genome-wide depletion of 5mC (Figure 1A) and instead clarifies the model to demonstrate that Tet1 and Tet2 function to regulate locus-specific methylation during PGC development.

EXPERIMENTAL PROCEDURES

Embryonic Stem Cell Culture and iPGC Differentiation

Mouse ESC maintenance, differentiation, and isolation of iPGCs were performed as previously described (Vincent et al., 2011). For the Tet studies, lentiviruses were modified from Ambartsumyan et al., 2010, to carry shRNA directed against *Tet1* mRNA harboring hygromycin resistance. Cells were transduced with the indicated VSV-G pseudotyped virus at a multiplicity of infection of 1 and selected in 200 μg/ml hygromycin on inactivated DR4 mouse embryonic fibroblasts. EB differentiation was performed with hygromycin in the media for 6 days prior to FACS.

Mouse Studies

Oct4-GFP^{+} embryos were used to isolate PGCs by FACS, as previously described (Vincent et al., 2011). All research protocols were approved by the Animal Care and Use Committee at UCLA.

Single-Cell PCR

Single-cell analysis was performed with the use of the Fluidigm BioMark microfluidics PCR system, as previously described, and involved an 18 cycle Specific Target Amplification reaction (Vincent et al., 2011). Heatmaps of Ct values were generated with Fluidigm PCR data analysis software.

Whole-Genome Bisulfite Sequencing

BS-seq libraries were prepared as previously described (Feng et al., 2011). Libraries were all single-end reads containing premethylated illumina adaptors. Libraries were sequenced on either a Genome Analyzer II or HiSeq 2000 and the percent methylation did not change between machines. Mapping was performed with the use of BS Seeker, and methylation levels for each cytosine were determined by measuring the ratio of Cs to Cs plus Ts that align to each genomic cytosine (Chen et al., 2010). Read lengths ranged from 50 to 80 after trimming 20 bases from the 3′ end. Multiple reads mapped to the same location were considered only once. For deep sequencing of libraries mB557 and mB556 (Table S1), only cytosines with coverage ≥ 4 were included for the downstream analysis (478,482,437 cytosines). This set was used to acquire chromosome views, metaplots, Shannon entropy, distribution plots, and analysis of symmetry. To generate a metaplot of genes, the transcription start and end sites of selected genes were fixed and the upstream, body, and downstream regions were binned into windows. For each window, the average methylation level was calculated. Therefore, a metagene plot summarized the average methylation level per window and was plotted from the upstream to downstream direction. Shannon entropy was calculated $-\sum_i^n m_i\, Log(m_i)$, where m_i is the methylation levels estimated at the i-th CG site. In the comparison, we took the average of Shannon entropy (i.e., divided by n). To map DMS CG, sites were selected with the use of the criteria of delta methylation levels $\geq 30\%$ and subjected to two-way binomial tests. This yielded 11,994,107 CG sites for analysis with a false discovery rate (FDR) of $\leq 5\%$. In the scatter plots, the points show the Δ methylation level between the two samples versus the changes of expression (log2 microarray 1–log2 microarray 2). Distribution plots of methylation levels were calculated at each cytosine as the ratio of Cs to Cs plus Ts that align to each genomic cytosine. The methylation levels of all cytosines with coverage $\geq 4\times$ were plotted as a histogram. To calculate symmetry, the methylation status of these cytosines is based on an FDR of 1% and a sequencing error of 1% (Lister et al., 2009). As a result, the methylation status (methylated or not methylated) of all eligible cytosines were determined by counting the numbers of both methylated (mC+mG), one methylated and one unmethylated (mC+uG), and both unmethylated (uC+uG) among CpG pairs in mBS48 and mBS49. For analysis of Tet2$^{-/-}$; LV and Tet2$^{-/-}$; Tet1shLV samples, n = 3 libraries were prepared in biological triplicate in samples that exhibited knockdown of Tet1 that was $\geq 69\%$ of the Tet2$^{-/-}$; control sample. This analysis yielded 6,866,888 CG dinucleotides that were represented in all six libraries and used to calculate the percent of CG methylation. We used t tests to calculate the significance between two groups.

LC-ESI-MS/MS-MRM

DNA was extracted from freshly sorted cell populations by FACS with a Zymo Quick-gDNA MiniPrep kit, and LC-ESI-MS/MS-MRM was used to determine the proportional content of 5mC or 5hmC relative to total cytosine levels, according to Le et al., 2011.

Immunofluorescence

Paraffin-embedded tissue staining was performed with conventional protocols with some exceptions. For 5mC and 5hmC staining, tissue was first stained for other markers, postfixed, and denatured for 10 min in 4 N HCl prior to overnight incubation with the appropriate antibodies. The following antibodies were used: Oct4 (Santa Cruz Biotechnology), E-cadherin (BD Biosciences), SSEA1 (Developmental Studies Hybridoma Bank), 5mC (Aviva Biosciences), and 5hmC (Active Motif). Fluorescent visualization was performed with the use of isotype-specific secondary antibodies conjugated to either fluorescein isothiocyanate or Alexa Fluor 594 (Jackson ImmunoResearch). All images were acquired on a Zeiss LSM 780 confocal microscope.

ACCESSION NUMBERS

All BS-seq data reported have been uploaded to the Gene Expression Omnibus (GEO) at accession number GSE44092.

SUPPLEMENTAL INFORMATION

Supplemental Information contains two figures and two tables and can be found with this article online at http://dx.doi.org/10.1016/j.stem.2013.01.016.

ACKNOWLEDGMENTS

This work is supported by grant R01HD058047 from the National Institutes of Health (NIH) and a Research Award from the Eli and Edythe Broad Center for Regenerative Medicine and Stem Cell Research to A.T.C. and NIH grants R01 HD065812 and CA151535 to A.R. The sequencing and FACS experiments were performed at the Eli and Edythe Broad Center for Regenerative Medicine and Stem Cell Research Sequencing Center and FACS facility. J.J.V. is supported by a Dissertation Year Fellowship from UCLA. Y.H. and S.F. are supported by postdoctoral fellowships from the Leukemia & Lymphoma Society and J.H.C. is supported by fellowship TG2-01169 from the California Institute for Regenerative Medicine. Requests for *Tet2*$^{-/-}$ ESCs should be directed to A.R. at the La Jolla Institute for Allergy and Immunology, La Jolla, CA, USA.

Received: December 10, 2012
Revised: January 21, 2013
Accepted: January 27, 2013
Published: February 14, 2013

REFERENCES

Ambartsumyan, G., Gill, R.K., Perez, S.D., Conway, D., Vincent, J., Dalal, Y., and Clark, A.T. (2010). Centromere protein A dynamics in human pluripotent stem cell self-renewal, differentiation and DNA damage. Hum. Mol. Genet. *19*, 3970–3982.

Bostick, M., Kim, J.K., Estève, P.O., Clark, A., Pradhan, S., and Jacobsen, S.E. (2007). UHRF1 plays a role in maintaining DNA methylation in mammalian cells. Science *317*, 1760–1764.

Carmell, M.A., Girard, A., van de Kant, H.J., Bourc'his, D., Bestor, T.H., de Rooij, D.G., and Hannon, G.J. (2007). MIWI2 is essential for spermatogenesis and repression of transposons in the mouse male germline. Dev. Cell *12*, 503–514.

Chen, P.Y., Cokus, S.J., and Pellegrini, M. (2010). BS Seeker: precise mapping for bisulfite sequencing. BMC Bioinformatics *11*, 203.

Dawlaty, M.M., Ganz, K., Powell, B.E., Hu, Y.C., Markoulaki, S., Cheng, A.W., Gao, Q., Kim, J., Choi, S.W., Page, D.C., and Jaenisch, R. (2011). Tet1 is dispensable for maintaining pluripotency and its loss is compatible with embryonic and postnatal development. Cell Stem Cell *9*, 166–175.

Feng, S., Cokus, S.J., Zhang, X., Chen, P.Y., Bostick, M., Goll, M.G., Hetzel, J., Jain, J., Strauss, S.H., Halpern, M.E., et al. (2010). Conservation and divergence of methylation patterning in plants and animals. Proc. Natl. Acad. Sci. USA *107*, 8689–8694.

Feng, S., Rubbi, L., Jacobsen, S.E., and Pellegrini, M. (2011). Determining DNA methylation profiles using sequencing. Methods Mol. Biol. *733*, 223–238.

Ficz, G., Branco, M.R., Seisenberger, S., Santos, F., Krueger, F., Hore, T.A., Marques, C.J., Andrews, S., and Reik, W. (2011). Dynamic regulation of 5-hydroxymethylcytosine in mouse ES cells and during differentiation. Nature *473*, 398–402.

Gkountela, S., Li, Z., Vincent, J.J., Zhang, K.X., Chen, A., Pellegrini, M., and Clark, A.T. (2012). The ontogeny of cKIT(+) human primordial germ cells proves to be a resource for human germ line reprogramming, imprint erasure and in vitro differentiation. Nat. Cell Biol. *15*, 113–122.

Guibert, S., Forné, T., and Weber, M. (2012). Global profiling of DNA methylation erasure in mouse primordial germ cells. Genome Res. *22*, 633–641.

Hackett, J.A., Sengupta, R., Zylicz, J.J., Murakami, K., Lee, C., Down, T.A., and Surani, M.A. (2013). Germline DNA demethylation dynamics and imprint erasure through 5-hydroxymethylcytosine. Science *339*, 448–452.

Hajkova, P., Erhardt, S., Lane, N., Haaf, T., El-Maarri, O., Reik, W., Walter, J., and Surani, M.A. (2002). Epigenetic reprogramming in mouse primordial germ cells. Mech. Dev. *117*, 15–23.

Hajkova, P., Ancelin, K., Waldmann, T., Lacoste, N., Lange, U.C., Cesari, F., Lee, C., Almouzni, G., Schneider, R., and Surani, M.A. (2008). Chromatin dynamics during epigenetic reprogramming in the mouse germ line. Nature *452*, 877–881.

Hajkova, P., Jeffries, S.J., Lee, C., Miller, N., Jackson, S.P., and Surani, M.A. (2010). Genome-wide reprogramming in the mouse germ line entails the base excision repair pathway. Science *329*, 78–82.

Huang, Y., Pastor, W.A., Shen, Y., Tahiliani, M., Liu, D.R., and Rao, A. (2010). The behaviour of 5-hydroxymethylcytosine in bisulfite sequencing. PLoS ONE *5*, e8888.

Iqbal, K., Jin, S.G., Pfeifer, G.P., and Szabó, P.E. (2011). Reprogramming of the paternal genome upon fertilization involves genome-wide oxidation of 5-methylcytosine. Proc. Natl. Acad. Sci. USA *108*, 3642–3647.

Kafri, T., Ariel, M., Brandeis, M., Shemer, R., Urven, L., McCarrey, J., Cedar, H., and Razin, A. (1992). Developmental pattern of gene-specific DNA methylation in the mouse embryo and germ line. Genes Dev. *6*, 705–714.

Koh, K.P., Yabuuchi, A., Rao, S., Huang, Y., Cunniff, K., Nardone, J., Laiho, A., Tahiliani, M., Sommer, C.A., Mostoslavsky, G., et al. (2011). Tet1 and Tet2 regulate 5-hydroxymethylcytosine production and cell lineage specification in mouse embryonic stem cells. Cell Stem Cell *8*, 200–213.

Laird, C.D., Pleasant, N.D., Clark, A.D., Sneeden, J.L., Hassan, K.M., Manley, N.C., Vary, J.C., Jr., Morgan, T., Hansen, R.S., and Stöger, R. (2004). Hairpin-bisulfite PCR: assessing epigenetic methylation patterns on complementary strands of individual DNA molecules. Proc. Natl. Acad. Sci. USA *101*, 204–209.

Lane, N., Dean, W., Erhardt, S., Hajkova, P., Surani, A., Walter, J., and Reik, W. (2003). Resistance of IAPs to methylation reprogramming may provide a mechanism for epigenetic inheritance in the mouse. Genesis *35*, 88–93.

Lawson, K.A., and Hage, W.J. (1994). Clonal analysis of the origin of primordial germ cells in the mouse. Ciba Found. Symp. *182*, 68–91.

Le, T., Kim, K.P., Fan, G., and Faull, K.F. (2011). A sensitive mass spectrometry method for simultaneous quantification of DNA methylation and hydroxymethylation levels in biological samples. Anal. Biochem. *412*, 203–209.

Lees-Murdock, D.J., De Felici, M., and Walsh, C.P. (2003). Methylation dynamics of repetitive DNA elements in the mouse germ cell lineage. Genomics *82*, 230–237.

Lei, H., Oh, S.P., Okano, M., Jüttermann, R., Goss, K.A., Jaenisch, R., and Li, E. (1996). De novo DNA cytosine methyltransferase activities in mouse embryonic stem cells. Development *122*, 3195–3205.

Lister, R., Pelizzola, M., Dowen, R.H., Hawkins, R.D., Hon, G., Tonti-Filippini, J., Nery, J.R., Lee, L., Ye, Z., Ngo, Q.M., et al. (2009). Human DNA methylomes at base resolution show widespread epigenomic differences. Nature *462*, 315–322.

Monk, M., Boubelik, M., and Lehnert, S. (1987). Temporal and regional changes in DNA methylation in the embryonic, extraembryonic and germ cell lineages during mouse embryo development. Development *99*, 371–382.

Ohinata, Y., Seki, Y., Payer, B., O'Carroll, D., Surani, M.A., and Saitou, M. (2006). Germline recruitment in mice: a genetic program for epigenetic reprogramming. Ernst Schering Res. Found. Workshop *60*, 143–174.

Okano, M., Bell, D.W., Haber, D.A., and Li, E. (1999). DNA methyltransferases Dnmt3a and Dnmt3b are essential for de novo methylation and mammalian development. Cell *99*, 247–257.

Popp, C., Dean, W., Feng, S., Cokus, S.J., Andrews, S., Pellegrini, M., Jacobsen, S.E., and Reik, W. (2010). Genome-wide erasure of DNA methylation in mouse primordial germ cells is affected by AID deficiency. Nature *463*, 1101–1105.

Reik, W., and Walter, J. (2001). Genomic imprinting: parental influence on the genome. Nat. Rev. Genet. *2*, 21–32.

Seisenberger, S., Andrews, S., Krueger, F., Arand, J., Walter, J., Santos, F., Popp, C., Thienpont, B., Dean, W., and Reik, W. (2012). The Dynamics of Genome-wide DNA Methylation Reprogramming in Mouse Primordial Germ Cells. Mol. Cell *48*, 849–862.

Seki, Y., Hayashi, K., Itoh, K., Mizugaki, M., Saitou, M., and Matsui, Y. (2005). Extensive and orderly reprogramming of genome-wide chromatin modifications associated with specification and early development of germ cells in mice. Dev. Biol. *278*, 440–458.

Smith, Z.D., Chan, M.M., Mikkelsen, T.S., Gu, H., Gnirke, A., Regev, A., and Meissner, A. (2012). A unique regulatory phase of DNA methylation in the early mammalian embryo. Nature *484*, 339–344.

Tahiliani, M., Koh, K.P., Shen, Y., Pastor, W.A., Bandukwala, H., Brudno, Y., Agarwal, S., Iyer, L.M., Liu, D.R., Aravind, L., and Rao, A. (2009). Conversion of 5-methylcytosine to 5-hydroxymethylcytosine in mammalian DNA by MLL partner TET1. Science *324*, 930–935.

Tam, P.P., and Zhou, S.X. (1996). The allocation of epiblast cells to ectodermal and germline lineages is influenced by the position of the cells in the gastrulating mouse embryo. Dev. Biol. *178*, 124–132.

Tanaka, T., Hosokawa, M., Vagin, V.V., Reuter, M., Hayashi, E., Mochizuki, A.L., Kitamura, K., Yamanaka, H., Kondoh, G., Okawa, K., et al. (2011). Tudor domain containing 7 (Tdrd7) is essential for dynamic ribonucleoprotein (RNP) remodeling of chromatoid bodies during spermatogenesis. Proc. Natl. Acad. Sci. USA *108*, 10579–10584.

Vincent, J.J., Li, Z., Lee, S.A., Liu, X., Etter, M.O., Diaz-Perez, S.V., Taylor, S.K., Gkountela, S., Lindgren, A.G., and Clark, A.T. (2011). Single cell analysis facilitates staging of Blimp1-dependent primordial germ cells derived from mouse embryonic stem cells. PLoS ONE *6*, e28960.

Yabuta, Y., Ohta, H., Abe, T., Kurimoto, K., Chuma, S., and Saitou, M. (2011). TDRD5 is required for retrotransposon silencing, chromatoid body assembly, and spermiogenesis in mice. J. Cell Biol. *192*, 781–795.

Yamaguchi, S., Hong, K., Liu, R., Shen, L., Inoue, A., Diep, D., Zhang, K., and Zhang, Y. (2012). Tet1 controls meiosis by regulating meiotic gene expression. Nature *492*, 443–447.

Ying, Y., Qi, X., and Zhao, G.Q. (2001). Induction of primordial germ cells from murine epiblasts by synergistic action of BMP4 and BMP8B signaling pathways. Proc. Natl. Acad. Sci. USA *98*, 7858–7862.